CRYSTAL GROWTH & DESIGN

pubs.acs.org/crystal

Communication

Octahedral Molybdenum Cluster-Based Single Crystals as Fabry–Pérot Microresonators

Elena Segura-Sanchis, Roberto Fenollosa,* Isabelle Rodriguez, Yann Molard, Stéphane Cordier, Marta Feliz,* and Pedro Atienzar*

Cite This: *Cryst. Growth Des.* 2022, 22, 60–65

Read Online

ACCESS | Metrics & More | Article Recommendations | Supporting Information

ABSTRACT: Single crystals built up from octahedral Mo_6 cluster units, with appropriate geometry and size, constitute Fabry–Pérot-type optical microcavities with well-defined resonances. Such resonances appear in the VIS-NIR range when performing optical transmittance (OT) or photoluminescence (PL) measurements. They strongly depend on the crystal thickness and on the optical constants of the material, specifically the real and imaginary parts of the refractive index. In this work, the accurate measurement of the crystal thickness is used for the determination of the optical constants by means of a fitting process, and the preferred orientation of the crystals was determined by X-ray diffraction.

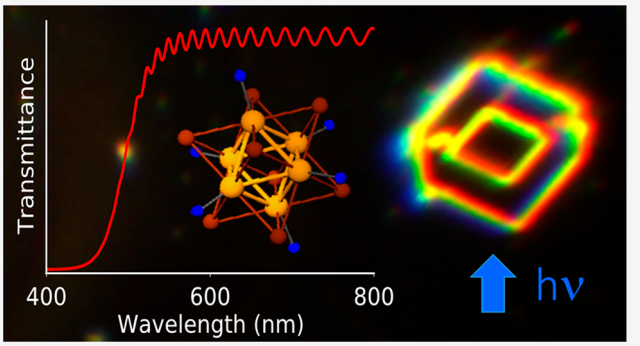

In the past decades, octahedral molybdenum clusters have attracted increasing attention from the scientific community due to their intrinsic photophysical and redox properties. These clusters are found in complexes with the general formula $[Mo_6X^i_8L^a_6]^n$ ($-2 \leq n \leq 4$), where X^i are inner halide ligands and L^a correspond to organic or inorganic apical (or terminal) ligands. These clusters have outstanding optical properties such as absorption of light in the UV–vis range, bright emission in the red/near-IR region with high quantum yields, and PL lifetimes up to several hundreds of microseconds.[1−4] It is also well-known that these clusters act as efficient photosensitizers in processes related to the generation of singlet oxygen. These properties make these inorganic compounds particularly attractive in design of functional hybrid nanomaterials with potential applications in nano-architectonics,[5,6] optoelectronics,[7−20] lighting,[21] hydrogen storage,[22] biomedicine,[4,23−32] and catalysis.[33−44] Surprisingly, only scarce studies about the optical and electronic properties of octahedral molybdenum cluster-based materials at the single crystal level and at the micrometer scale are reported, and those are limited to $Cs_2[Mo_6X^i_8X^a_6]$ (X = Cl, Br, I) compounds.[45−51]

Getting single crystals at the micrometer and nanometer scales is advantageous for device manufacturing in the development of high-efficiency solar cells, photonic and optoelectronic devices, sensors, and photocatalysts. The difficulties of growing bigger crystals are avoided, and a low defect density and interferences from the grain boundaries are expected. One area of great interest for applications in optics and sensing is the use of single crystal materials as Fabry–Pérot microresonators. Fabry–Pérot cavities are fundamental and ubiquitous optical elements frequently used in many important devices, such as lasers or narrowband wavelength filters in spectrometers.[52−57] In this sense, it is crucial to study deeply the intrinsic optical properties of molybdenum cluster-based materials at the single crystal level. While the molybdenum cluster composition determines the refractive index, the shape of crystals provides the type of attainable optical modes. Both a high refractive index and a geometry with parallel facets are expected to favor the appearance of Fabry–Pérot resonances. As far as we know, the refractive index of octahedral-based cluster materials was only reported twice: first, for immobilized $[Mo_6I^i_8]^{4+}$ cluster cores onto *p*- and *n*-doped Si(111) surfaces through complexation by a pyridine-terminated organic monolayer previously covalently bound to hydrogen-terminated Si(111).[58] In that study, an increase of the real part of the refractive index (n) of the pyridine-terminated Si(111) monolayer was observed after the molybdenum cluster immobilization (from 1.67 ± 0.03 to 1.79 ± 0.02, respectively). The Brewster angle technique was also used to determine the real part of the refractive index at 650 nm of a polydimethylsiloxane (PDMS) doped with 2 wt % of a $[Mo_6I_8(OCOC_2F_5)_6]^{2-}$ cluster anion and 0.5 wt % of a blue–green emissive organic luminophore.[9] In this case, the increase

Received: October 1, 2021
Revised: November 24, 2021
Published: December 2, 2021

https://doi.org/10.1021/acs.cgd.1c01144
Cryst. Growth Des. 2022, 22, 60–65

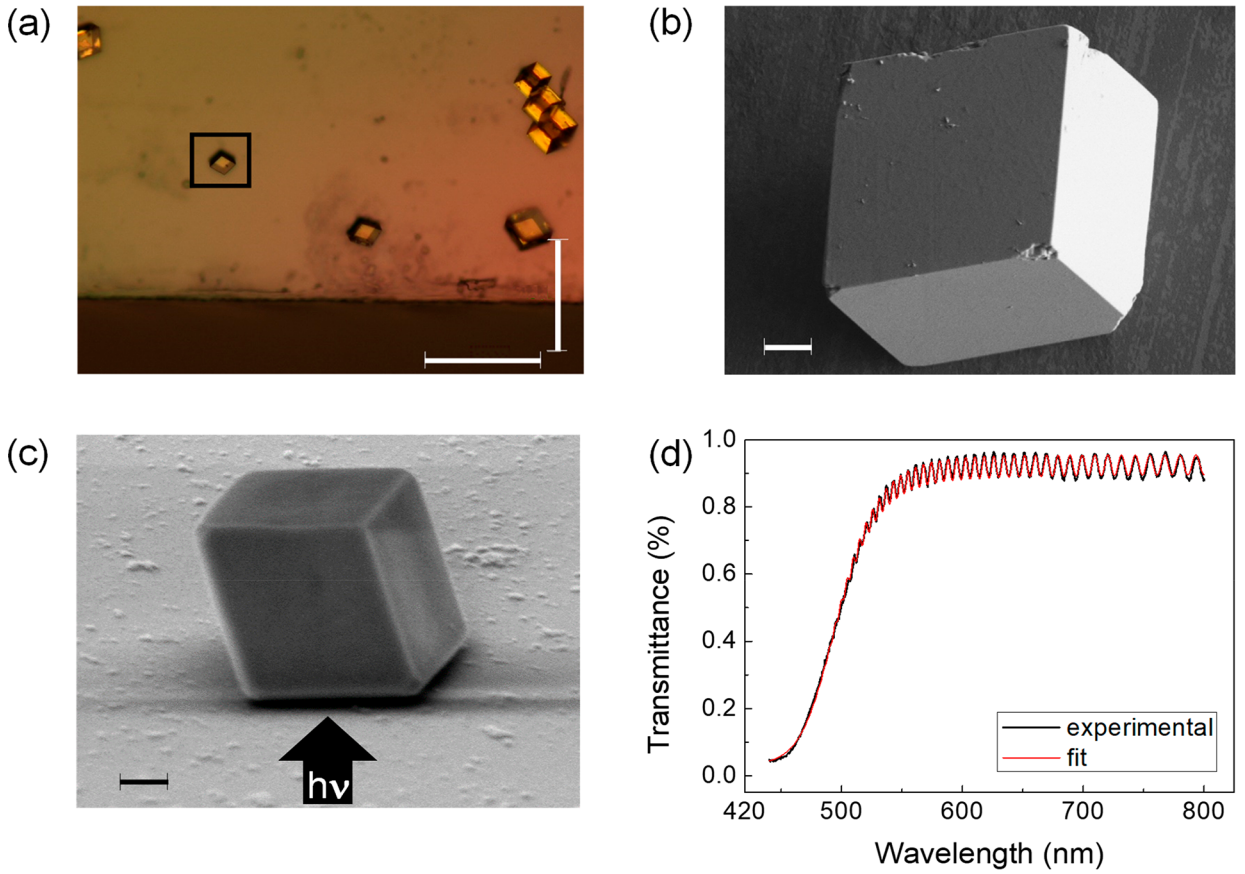

Figure 1. Optical microscopy of several crystals of **MC** deposited on a glass substrate (a), FESEM images of the top view (b) and cross-sectional view (c) of two crystals, and experimental and fitted OT spectra (d) of the selected crystal in (a) measured in the direction indicated by the arrow in (c). Scale bars in (a) 100 μm; in (b,c) 1 μm.

of n from 1.42 up to 1.48 upon doping allows waveguiding propagation under perpendicular or longitudinal excitation of the emitted white light in a silica microfiber containing the doped polymer.

We have previously reported the synthesis of $(H_3O)_2[Mo_6Br^i_8(OH)^a_6]\cdot 10H_2O$ (**MC**) single crystals by hydrolysis of the $(TBA)_2[Mo_6Br^i_8F^a_6]$ (TBA = tetrabutylammonium) precursor.[42] The chemical composition was confirmed by XPS and EDX-SEM analyses. The Raman spectrum showed the characteristic band shifts of the Mo_6 cluster based unit. The structure of **MC** was determined by single crystal X-ray diffraction. It crystallizes in the $R\bar{3}m$ space group (no. 166) with the following unit cell parameters: a = 15.2455(8) Å, c = 11.1440(8). Schematically, the structure can be depicted as the stacking of $[Mo_6Br^i_8(OH)^a_6]^{2-}$ cluster units according to a A−B−C−A mode. Water molecules are ordered and located within the voids generated by the cluster unit stacking. It is worth noting that a strong hydrogen-bond network develops between the clusters and the water molecules.[15] The latter is magnified by the presence of protons that counter balance the charge of the cluster unit. They are statistically shared by apical hydroxyl groups between adjacent clusters leading to protonic conductivity. This crystalline material remains, until now, the highest active catalyst in the light-driven water reduction to molecular hydrogen among the Mo_6-cluster based materials tested, achieving productions up to 4298 μmol g^{-1} catalyst of H_2 after 5 h of illumination.[42] The optical studies of these cluster single crystals are limited to PL, showing the characteristic cluster emission in the red region of the spectrum.

Herein, we controlled the growth and isolated single crystals of **MC** with different crystal sizes. Herein the possibility to use these crystals as optical cavities for potential applications in photonic technologies is shown. This molybdenum cluster-based material was studied with a homemade optical system, and the crystal emission and transmittance spectra were analyzed in order to extract the optical constants of the material.[59]

The preparation of single crystals with composition **MC** was optimized by cautious control of the crystallization conditions to obtain the targeted size.[42] Single crystals of **MC** were obtained with regular shapes, parallel faces, and with density of defects with a yield around 90%. The remaining material was associated with some agglomerates and irregular particles. Small-sized (less than 30 μm) crystals were selected, and their morphology was studied. Figures 1a and S1 (see Supporting Information) show the optical microscopy images of several crystals supported on a glass substrate. The top view and cross section field-emission scanning electron microscopy (FESEM) images for the collected single crystals (Figure 1b and c, respectively) reveal a rhombohedral crystal habit with average crystal faces with angles of 107.4° and 71.9° for crystals with sizes between ca. 15 and 5 μm. At this degree of magnification, some defects and small attached particles were detected from the chosen specimen.

Aiming to study the orientation of the deposited single crystals, the X-ray pattern of few single crystals dispersed onto

https://doi.org/10.1021/acs.cgd.1c01144
Cryst. Growth Des. 2022, 22, 60−65

a Si(911) substrate was recorded. Five diffraction peaks are identified in the diffractogram (Figure S2, Supporting Information) and correspond to the family of planes in the $\{\bar{1}11\}$ direction, with an interplanar distance between peaks of 8.516 Å, on the basis of the symmetry of the single crystals. This unique disposition of the $\{\bar{1}11\}$ facets confirms a preferential orientation of the single crystals, resting on their flat surfaces upon deposition onto a surface. The X-ray patterns acquired after optical studies remained unaltered (Figure 2) which confirms the single crystal stability under light irradiation with standard measurement conditions.

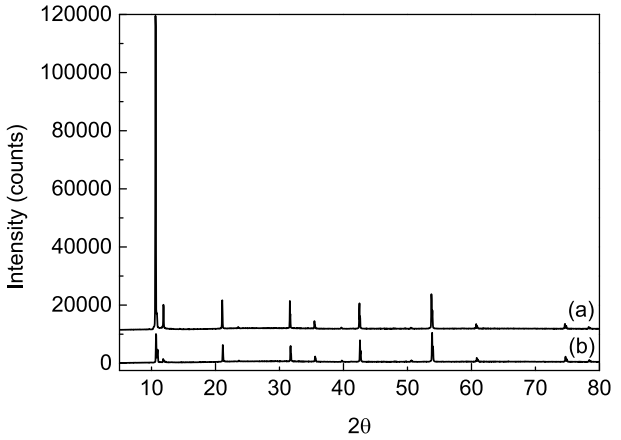

Figure 2. X-ray patterns of a set of single crystals of **MC** before (a) and after (b) optical studies.

The thermogravimetric/differential thermal analysis (TG/DTA) registered for the crystalline samples of **MC** also probe their thermal stability under operational conditions. The TG/DTA curves (Figure S3, Supporting Information) obtained under dry atmosphere show that the crystals remain stable up to 63 °C. This thermal stability confirms their potential applications as optical microcavities. At higher temperatures (63−81 °C), the sample displays a weight loss of 14% that we associate with water molecules, and this could be responsible for a structural reorganization of the crystals.

Flat and clean facets are convenient for observing optical resonances. A clear resonance phenomenon was observed in most of the crystals analyzed, in spite of the fact that some of them had defects and, eventually, other smaller attached particles. Figure 1d shows the OT spectrum measured in the direction perpendicular to the supporting substrate of the single crystal selected in Figure 1a. The spectrum consists of two different regions. One region at shorter wavelengths (from 425 to ca. 550 nm) is characterized by an abrupt transition from vanishing to high transmittance. The strong absorption of the material observed in the diffuse reflectance spectrum in this wavelength range (Figure S3, Supporting Information) prevents the optical resonance phenomenon. The second region, displayed in the range from ca. 550 nm to longer wavelengths, shows a low absorption and clear interference fringes, which indicate that the crystal behaves as an optical microcavity. Such fringes depend basically on two parameters: refractive index and crystal thickness.[60] Thus, for a given refractive index dispersion, the thinner the crystal is, the more separated the fringes.[61] Such parameters can be deduced by fitting the transmittance spectrum to an appropriate model (see Supporting Information). However, it is convenient to determine the crystal thickness by other means first in order to avoid spurious solutions. Figure 1d illustrates the fitted spectrum to a reported model[59] for a crystal thickness, determined by optical profilometry of (13 650 ± 50) nm. Figure 3a,b shows the respective fitted real (n) and imaginary (k) parts of the refractive index. The real part of the refractive index is comparable to those reported for other molybdenum materials, such as molybdenum oxide films, that usually appear in the range of 1.7−2.3.[62−66] The error in the measurement of the thickness yields, in the case of n, a confidence interval indicated by the gray area (Figure 3a). Regarding k, the fitted values should be considered cautiously because OT measurements include most probably optical scattering, which cannot be distinguished from optical absorption, and it was not considered in the fitting model. As another example, Figure S4 (see Supporting Information) shows the OT measurement of a crystal of (15 800 ± 50) nm in thickness and the fit to the same model.[59] Figure S5a,b (see Supporting Information) shows the corresponding fitted real and imaginary parts, respectively, of the refractive index (red curves). For comparison, the fitted values for the sample of Figure 1 are plotted in black in Figure S5 (Supporting Information). While the values almost coincide in the case of the real part, large discrepancies arise for the imaginary part, especially in the short-wavelength region. This is not surprising, and it is

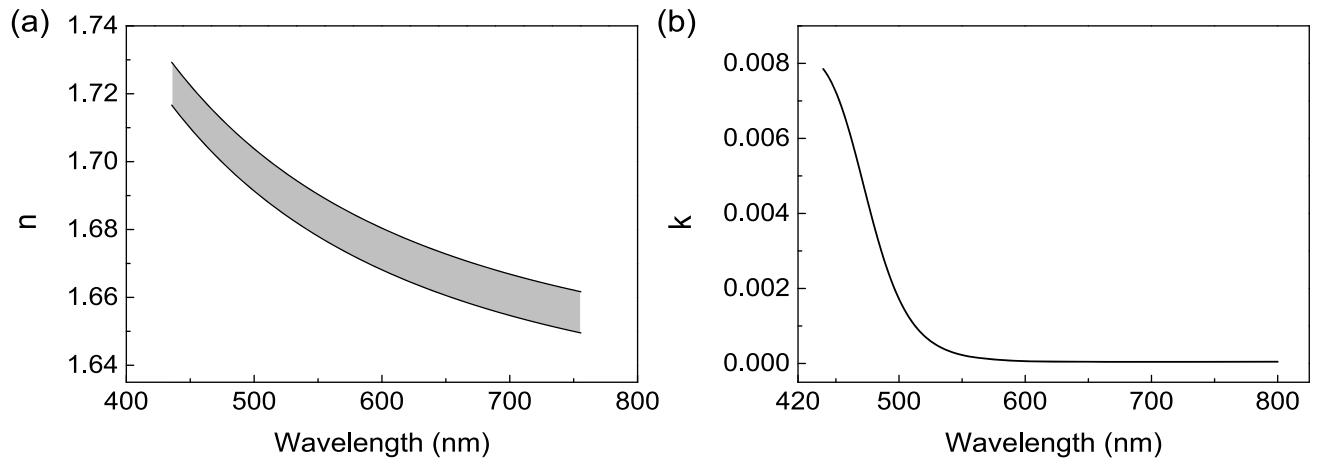

Figure 3. Fitted real (a) and imaginary (b) parts of the refractive index for the crystal selected in Figure 1(a).

https://doi.org/10.1021/acs.cgd.1c01144
Cryst. Growth Des. 2022, 22, 60−65

attributed to imponderable optical scattering, which depends on the crystal size, the light spot size, and its position on the crystal.

Single crystals of **MC** yielded PL when they were excited in the absorption region (Figure S6, Supporting Information), and the emission properties have been previously reported (λ_{em} = 670 nm, λ_{exc} = 390−430 nm).[42] Such PL can couple to the optical resonance modes of the cavity and produces interference fringes as well. However, because of the envelope curve, they are more difficult to observe than in the case of the OT signal. Figure 4 shows a crystal (see inset) of (10 500 ± 50) nm in thickness where both OT and PL were measured. It is important to stress that the spectral position of the resonances is the same for both spectra.

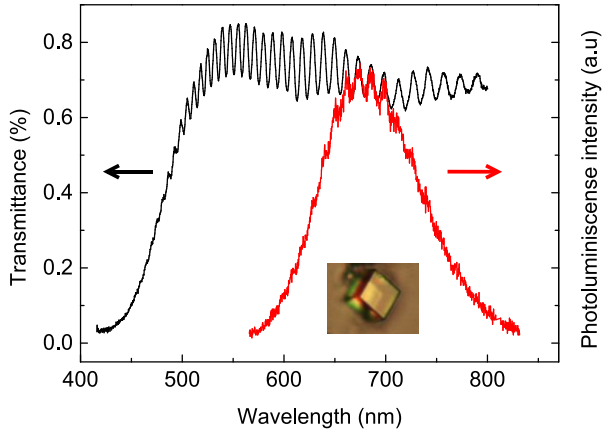

Figure 4. OT (black) and PL (red) spectra of the crystal shown in the inset.

In summary, high-quality single crystals of **MC** deposited with a preferred orientation onto a flat surface showed well-defined resonances in the VIS-NIR range when OT or PL measurements were done in a perpendicular direction to the surface. We have proven that selected Mo_6 cluster-based crystals constitute Fabry−Pérot-type optical microcavities with potential applications in photonic devices.

■ ASSOCIATED CONTENT

Supporting Information

The Supporting Information is available free of charge at https://pubs.acs.org/doi/10.1021/acs.cgd.1c01144.

Experimental details including the preparation of single crystals, the instrumentation and the fitting model used for the optical transmittance, and supplementary figures (PDF)

■ AUTHOR INFORMATION

Corresponding Authors

Roberto Fenollosa − *Instituto de Tecnología Química (Universitat Politècnica de València − Consejo Superior de Investigaciones Científicas), 46022 Valencia, Spain;* orcid.org/0000-0003-2758-9823; Email: rfenollo@ter.upv.es

Marta Feliz − *Instituto de Tecnología Química (Universitat Politècnica de València − Consejo Superior de Investigaciones Científicas), 46022 Valencia, Spain;* orcid.org/0000-0002-4429-0551; Email: mfeliz@itq.upv.es

Pedro Atienzar − *Instituto de Tecnología Química (Universitat Politècnica de València − Consejo Superior de Investigaciones Científicas), 46022 Valencia, Spain;* orcid.org/0000-0002-0356-021X; Email: pedatcor@itq.upv.es

Authors

Elena Segura-Sanchis − *Instituto de Tecnología Química (Universitat Politècnica de València − Consejo Superior de Investigaciones Científicas), 46022 Valencia, Spain*

Isabelle Rodriguez − *Instituto de Tecnología Química (Universitat Politècnica de València − Consejo Superior de Investigaciones Científicas), 46022 Valencia, Spain;* orcid.org/0000-0001-5479-2494

Yann Molard − *Université de Rennes, CNRS, ISCR − UMR 6226, ScanMAT − UMS 2001, F-35000 Rennes, France;* orcid.org/0000-0002-6295-0883

Stéphane Cordier − *Université de Rennes, CNRS, ISCR − UMR 6226, ScanMAT − UMS 2001, F-35000 Rennes, France;* orcid.org/0000-0003-0707-3774

Complete contact information is available at: https://pubs.acs.org/10.1021/acs.cgd.1c01144

Notes

The authors declare no competing financial interest.

■ ACKNOWLEDGMENTS

This research was funded by the Severo Ochoa Program (grant number SEV-2016-0683), Ministerio de Ciencia e Innovación (grant number PGC2018-099744), and Generalitat Valenciana (grant number AICO/2020/149). The authors also thank the Electron Microscopy Service of the Universitat Politècnica de Valencia for their support in FESEM image acquisition.

■ REFERENCES

(1) Kirakci, K.; Kubat, P.; Langmaier, J.; Polivka, T.; Fuciman, M.; Fejfarova, K.; Lang, K. A. Comparative Study of the Redox and Excited State Properties of $(nBu_4N)_2[Mo_6X_{14}]$ and $(nBu_4N)_2[Mo_6X_8(CF_3COO)_6]$ (X = Cl, Br, or I). *Dalt. Trans.* **2013**, *42*, 7224−7232.

(2) Mikhaylov, M. A.; Sokolov, M. N. Molybdenum Iodides − from Obscurity to Bright Luminescence. *Eur. J. Inorg. Chem.* **2019**, *2019*, 4181−4197.

(3) Mikhailov, M. A.; Brylev, K. A.; Abramov, P. A.; Sakuda, E.; Akagi, S.; Ito, A.; Kitamura, N.; Sokolov, M. N. Synthetic Tuning of Redox, Spectroscopic, and Photophysical Properties of {Mo6I8}4+ Core Cluster Complexes by Terminal Carboxylate Ligands. *Inorg. Chem.* **2016**, *55*, 8437−8445.

(4) Evtushok, D. V.; Melnikov, A. R.; Vorotnikova, N. A.; Vorotnikov, Y. A.; Ryadun, A. A.; Kuratieva, N. V.; Kozyr, K. V.; Obedinskaya, N. R.; Kretov, E. I.; Novozhilov, I. N.; Mironov, Y. V.; Stass, D. V.; Efremova, O. A.; Shestopalov, M. A. A Comparative Study of Optical Properties and X-Ray Induced Luminescence of Octahedral Molybdenum and Tungsten Cluster Complexes. *Dalt. Trans.* **2017**, *46*, 11738−11747.

(5) Cordier, S.; Grasset, F.; Molard, Y.; Amela-Cortes, M.; Boukherroub, R.; Ravaine, S.; Mortier, M.; Ohashi, N.; Saito, N.; Haneda, H. Inorganic Molybdenum Octahedral Nanosized Cluster Units, Versatile Functional Building Block for Nanoarchitectonics. *J. Inorg. Organomet. Polym. Mater.* **2015**, *25*, 189−204.

(6) Molard, Y. Clustomesogens: Liquid Crystalline Hybrid Nanomaterials Containing Functional Metal Nanoclusters. *Acc. Chem. Res.* **2016**, *49*, 1514−1523.

(7) Truong, T. G.; Dierre, B.; Grasset, F.; Saito, N.; Saito, N.; Nguyen, T. K. N.; Takahashi, K.; Uchikoshi, T.; Amela-Cortes, M.;

Molard, Y.; Cordier, S.; Ohashi, N. Visible Tunable Lighting System Based on Polymer Composites Embedding ZnO and Metallic Clusters: From Colloids to Thin Films. *Sci. Technol. Adv. Mater.* **2016**, *17*, 443−453.
(8) Nguyen, N. T. K.; Renaud, A.; Dierre, B.; Bouteille, B.; Wilmet, M.; Dubernet, M.; Ohashi, N.; Grasset, F.; Uchikoshi, T. Extended Study on Electrophoretic Deposition Process of Inorganic Octahedral Metal Clusters: Advanced Multifunctional Transparent Nanocomposite Thin Films. *Bull. Chem. Soc. Jpn.* **2018**, *91*, 1763−1774.
(9) Khlifi, S.; Bigeon, J.; Amela-Cortes, M.; Dumait, N.; Akdas-Kiliç, H.; Taupier, G.; Freslon, S.; Cordier, S.; Derien, S.; Achard, M.; Loas, G.; Molard, Y. Poly(Dimethylsiloxane) Functionalized with Complementary Organic and Inorganic Emitters for the Design of White Emissive Waveguides. *J. Mater. Chem. C* **2021**, *9*, 7094−7102.
(10) Khlifi, S.; Bigeon, J.; Amela-Cortes, M.; Dumait, N.; Loas, G.; Cordier, S.; Molard, Y. Switchable Two-Dimensional Waveguiding Abilities of Luminescent Hybrid Nanocomposites for Active Solar Concentrators. *ACS Appl. Mater. Interfaces* **2020**, *12*, 14400−14407.
(11) Prévôt, M.; Amela-Cortes, M.; Manna, S. K.; Lefort, R.; Cordier, S.; Folliot, H.; Dupont, L.; Molard, Y. Design and Integration in Electro-Optic Devices of Highly Efficient and Robust Red-NIR Phosphorescent Nematic Hybrid Liquid Crystals Containing $[Mo_6I_8(OCOC_nF_{2n+1})_6]^{2-}$ (n = 1, 2, 3) Nanoclusters. *Adv. Funct. Mater.* **2015**, *25*, 4966−4975.
(12) Bigeon, J.; Huby, N.; Amela-Cortes, M.; Molard, Y.; Garreau, A.; Cordier, S.; Bêche, B.; Duvail, J.-L. Efficient Active Waveguiding Properties of Mo 6 Nano-Cluster-Doped Polymer Nanotubes. *Nanotechnology* **2016**, *27*, 255201.
(13) Nguyen, T. K. N.; Grasset, F.; Cordier, S.; Amela-Cortes, M.; Matsui, Y.; Ohashi, N.; Shirahata, N.; Uchikoshi, T. Preparation and Characterization of Hollow Silica Nanocomposite Functionalized with UV Absorbable Molybdenum Cluster. *Adv. Powder Technol.* **2020**, *31*, 895−903.
(14) Renaud, A.; Nguyen, T. K. N.; Grasset, F.; Raissi, M.; Guillon, V.; Delabrouille, F.; Dumait, N.; Jouan, P.-Y.; Cario, L.; Jobic, S.; Pellegrin, Y.; Odobel, F.; Cordier, S.; Uchikoshi, T. Preparation by Electrophoretic Deposition of Molybdenum Iodide Cluster-Based Functional Nanostructured Photoelectrodes for Solar Cells. *Electrochim. Acta* **2019**, *317*, 737−745.
(15) Daigre, G.; Cuny, J.; Lemoine, P.; Amela-Cortes, M.; Paofai, S.; Audebrand, N.; Le Gal La Salle, A.; Quarez, E.; Joubert, O.; Naumov, N. G.; Cordier, S. Metal Atom Clusters as Building Blocks for Multifunctional Proton-Conducting Materials: Theoretical and Experimental Characterization. *Inorg. Chem.* **2018**, *57*, 9814−9825.
(16) Renaud, A.; Grasset, F.; Dierre, B.; Uchikoshi, T.; Ohashi, N.; Takei, T.; Planchat, A.; Cario, L.; Jobic, S.; Odobel, F.; Cordier, S. Inorganic Molybdenum Clusters as Light-Harvester in All Inorganic Solar Cells: A Proof of Concept. *ChemistrySelect* **2016**, *1*, 2284−2289.
(17) Vorotnikov, Y. A.; Efremova, O. A.; Vorotnikova, N. A.; Brylev, K. A.; Edeleva, M. V.; Tsygankova, A. R.; Smolentsev, A. I.; Kitamura, N.; Mironov, Y. V.; Shestopalov, M. A. On the Synthesis and Characterisation of Luminescent Hybrid Particles: Mo_6 Metal Cluster Complex/SiO_2. *RSC Adv.* **2016**, *6*, 43367−43375.
(18) Nerambourg, N.; Aubert, T.; Neaime, C.; Cordier, S.; Mortier, M.; Patriarche, G.; Grasset, F. Multifunctional Hybrid Silica Nanoparticles Based on $[Mo_6Br_{14}]^{2-}$ Phosphorescent Nanosized Clusters, Magnetic γ-Fe_2O_3 and Plasmonic Gold Nanoparticles. *J. Colloid Interface Sci.* **2014**, *424*, 132−140.
(19) Dechézelles, J.-F.; Aubert, T.; Grasset, F.; Cordier, S.; Barthou, C.; Schwob, C.; Maître, A.; Vallée, R. A. L.; Cramail, H.; Ravaine, S. Fine Tuning of Emission through the Engineering of Colloidal Crystals. *Phys. Chem. Chem. Phys.* **2010**, *12*, 11993−11999.
(20) Grasset, F.; Dorson, F.; Cordier, S.; Molard, Y.; Perrin, C.; Marie, A.-M.; Sasaki, T.; Haneda, H.; Bando, Y.; Mortier, M. Water-in-Oil Microemulsion Preparation and Characterization of $Cs_2[Mo_6X_{14}]$@SiO_2 Phosphor Nanoparticles Based on Transition Metal Clusters (X = Cl,Br, and I). *Adv. Mater.* **2008**, *20*, 143−148.
(21) Robin, M.; Kuai, W.; Amela-Cortes, M.; Cordier, S.; Molard, Y.; Mohammed-Brahim, T.; Jacques, E.; Harnois, M. Epoxy Based Ink as Versatile Material for Inkjet-Printed Devices. *ACS Appl. Mater. Interfaces* **2015**, *7*, 21975−21984.
(22) Dybtsev, D.; Serre, C.; Schmitz, B.; Panella, B.; Hirscher, M.; Latroche, M.; Llewellyn, P. L.; Cordier, S.; Molard, Y.; Haouas, M.; Taulelle, F.; Férey, G. Influence of $[Mo_6Br_8F_6]^{2-}$ Cluster Unit Inclusion within the Mesoporous Solid MIL-101 on Hydrogen Storage Performance. *Langmuir* **2010**, *26*, 11283−11290.
(23) Vorotnikov, Y. A.; Pozmogova, T. N.; Solovieva, A. O.; Miroshnichenko, S. M.; Vorontsova, E. V.; Shestopalova, L. V.; Mironov, Y. V.; Shestopalov, M. A.; Efremova, O. A. Luminescent Silica Mesoparticles for Protein Transduction. *Mater. Sci. Eng., C* **2019**, *96*, 530−538.
(24) Brandhonneur, N.; Hatahet, T.; Amela-Cortes, M.; Molard, Y.; Cordier, S.; Dollo, G. Molybdenum Cluster Loaded PLGA Nanoparticles: An Innovative Theranostic Approach for the Treatment of Ovarian Cancer. *Eur. J. Pharm. Biopharm.* **2018**, *125*, 95−105.
(25) Elistratova, J.; Mukhametshina, A.; Kholin, K.; Nizameev, I.; Mikhailov, M.; Sokolov, M.; Khairullin, R.; Miftakhova, R.; Shammas, G.; Kadirov, M.; Petrov, K.; Rizvanov, A.; Mustafina, A. Interfacial Uploading of Luminescent Hexamolybdenum Cluster Units onto Amino-Decorated Silica Nanoparticles as New Design of Nanomaterial for Cellular Imaging and Photodynamic Therapy. *J. Colloid Interface Sci.* **2019**, *538*, 387−396.
(26) Cheplakova, A. M.; Solovieva, A. O.; Pozmogova, T. N.; Vorotnikov, Y. A.; Brylev, K. A.; Vorotnikova, N. A.; Vorontsova, E. V.; Mironov, Y. V.; Poveshchenko, A. F.; Kovalenko, K. A.; Shestopalov, M. A. Nanosized Mesoporous Metal−Organic Framework MIL-101 as a Nanocarrier for Photoactive Hexamolybdenum Cluster Compounds. *J. Inorg. Biochem.* **2017**, *166*, 100−107.
(27) Neaime, C.; Amela-Cortes, M.; Grasset, F.; Molard, Y.; Cordier, S.; Dierre, B.; Mortier, M.; Takei, T.; Takahashi, K.; Haneda, H.; Verelst, M.; Lechevallier, S. Time-Gated Luminescence Bioimaging with New Luminescent Nanocolloids Based on $[Mo_6I_8(C_2F_5COO)_6]^{2-}$ Metal Atom Clusters. *Phys. Chem. Chem. Phys.* **2016**, *18*, 30166−30173.
(28) Solovieva, A. O.; Vorotnikov, Y. A.; Trifonova, K. E.; Efremova, O. A.; Krasilnikova, A. A.; Brylev, K. A.; Vorontsova, E. V.; Avrorov, P. A.; Shestopalova, L. V.; Poveshchenko, A. F.; Mironov, Y. V.; Shestopalov, M. A. Cellular Internalisation, Bioimaging and Dark and Photodynamic Cytotoxicity of Silica Nanoparticles Doped by $\{Mo_6I_8\}^{4+}$ Metal Clusters. *J. Mater. Chem. B* **2016**, *4*, 4839−4846.
(29) Aubert, T.; Cabello-Hurtado, F.; Esnault, M.-A.; Neaime, C.; Lebret-Chauvel, D.; Jeanne, S.; Pellen, P.; Roiland, C.; Le Polles, L.; Saito, N.; Kimoto, K.; Haneda, H.; Ohashi, N.; Grasset, F.; Cordier, S. Extended Investigations on Luminescent $Cs_2[Mo_6Br_{14}]$@SiO_2 Nanoparticles: Physico-Structural Characterizations and Toxicity Studies. *J. Phys. Chem. C* **2013**, *117*, 20154−20163.
(30) Kirakci, K.; Kubát, P.; Fejfarová, K.; Martinčík, J.; Nikl, M.; Lang, K. X-Ray Inducible Luminescence and Singlet Oxygen Sensitization by an Octahedral Molybdenum Cluster Compound: A New Class of Nanoscintillators. *Inorg. Chem.* **2016**, *55*, 803−809.
(31) Kirakci, K.; Zelenka, J.; Rumlová, M.; Cvačka, J.; Ruml, T.; Lang, K. Cationic Octahedral Molybdenum Cluster Complexes Functionalized with Mitochondria-Targeting Ligands: Photodynamic Anticancer and Antibacterial Activities. *Biomater. Sci.* **2019**, *7*, 1386−1392.
(32) Brandhonneur, N.; Boucaud, Y.; Verger, A.; Dumait, N.; Molard, Y.; Cordier, S.; Dollo, G. Molybdenum Cluster Loaded PLGA Nanoparticles as Efficient Tools against Epithelial Ovarian Cancer. *Int. J. Pharm.* **2021**, *592*, 120079.
(33) Nagashima, S.; Kamiguchi, S.; Chihara, T. Catalytic Reactions over Halide Cluster Complexes of Group 5−7 Metals. *Metals* **2014**, *4*, 235−313.
(34) Kamiguchi, S.; Nagashima, S.; Chihara, T. Characterization of Catalytically Active Octahedral Metal Halide Cluster Complexes. *Metals* **2014**, *4*, 84−107.
(35) Kumar, P.; Kumar, S.; Cordier, S.; Paofai, S.; Boukherroub, R.; Jain, S. L. Photoreduction of CO_2 to Methanol with Hexanuclear

https://doi.org/10.1021/acs.cgd.1c01144
Cryst. Growth Des. 2022, 22, 60−65

Molybdenum $[Mo_6Br_{14}]^{2-}$ Cluster Units under Visible Light Irradiation. *RSC Adv.* **2014**, *4*, 10420−10423.
(36) Puche, M.; García-Aboal, R.; Mikhaylov, M. A.; Sokolov, M. N.; Atienzar, P.; Feliz, M. Enhanced Photocatalytic Activity and Stability in Hydrogen Evolution of Mo6 Iodide Clusters Supported on Graphene Oxide. *Nanomaterials* **2020**, *10*, 1259.
(37) Kumar, S.; Khatri, O. P.; Cordier, S.; Boukherroub, R.; Jain, S. L. Graphene Oxide Supported Molybdenum Cluster: First Heterogenized Homogeneous Catalyst for the Synthesis of Dimethylcarbonate from CO_2 and Methanol. *Chem. - Eur. J.* **2015**, *21*, 3488−3494.
(38) Barras, A.; Cordier, S.; Boukherroub, R. Fast Photocatalytic Degradation of Rhodamine B over $[Mo_6Br_8(N_3)_6]^{2-}$ Cluster Units under Sun Light Irradiation. *Appl. Catal., B* **2012**, *123*−*124*, 1−8.
(39) Barras, A.; Das, M. R.; Devarapalli, R. R.; Shelke, M. V.; Cordier, S.; Szunerits, S.; Boukherroub, R. One-Pot Synthesis of Gold Nanoparticle/Molybdenum Cluster/Graphene Oxide Nanocomposite and Its Photocatalytic Activity. *Appl. Catal., B* **2013**, *130*−*131*, 270−276.
(40) Kumar, P.; Mungse, H. P.; Cordier, S.; Boukherroub, R.; Khatri, O. P.; Jain, S. L. Hexamolybdenum Clusters Supported on Graphene Oxide: Visible-Light Induced Photocatalytic Reduction of Carbon Dioxide into Methanol. *Carbon* **2015**, *94*, 91−100.
(41) Beltrán, A.; Mikhailov, M.; Sokolov, M. N.; Pérez-Laguna, V.; Rezusta, A.; Revillo, M. J.; Galindo, F. A Photobleaching Resistant Polymer Supported Hexanuclear Molybdenum Iodide Cluster for Photocatalytic Oxygenations and Photodynamic Inactivation of Staphylococcus Aureus. *J. Mater. Chem. B* **2016**, *4*, 5975−5979.
(42) Feliz, M.; Puche, M.; Atienzar, P.; Concepción, P.; Cordier, S.; Molard, Y. InSituGeneration of Active Molybdenum Octahedral Clusters for Photocatalytic Hydrogen Production from Water. *ChemSusChem* **2016**, *9*, 1963−1971.
(43) Feliz, M.; Atienzar, P.; Amela-Cortés, M.; Dumait, N.; Lemoine, P.; Molard, Y.; Cordier, S. Supramolecular Anchoring of Octahedral Molybdenum Clusters onto Graphene and Their Synergies in Photocatalytic Water Reduction. *Inorg. Chem.* **2019**, *58*, 15443−15454.
(44) Ivanova, M. N.; Vorotnikov, Y. A.; Plotnikova, E. E.; Marchuk, M. V.; Ivanov, A. A.; Asanov, I. P.; Tsygankova, A. R.; Grayfer, E. D.; Fedorov, V. E.; Shestopalov, M. A. Hexamolybdenum Clusters Supported on Exfoliated H-BN Nanosheets for Photocatalytic Water Purification. *Inorg. Chem.* **2020**, *59*, 6439−6448.
(45) Saito, N.; Lemoine, P.; Cordier, S.; Matsushita, Y.; Ohsawa, T.; Grasset, F.; Cross, J. S.; Ohashi, N. Structural and Electronic Properties of the Metal Cluster-Based Compounds Including High Concentration of Solvent Molecules. *Z. Anorg. Allg. Chem.* **2021**, *647*, 751−758.
(46) Saito, N.; Lemoine, P.; Dumait, N.; Amela-Cortes, M.; Paofai, S.; Roisnel, T.; Nassif, V.; Grasset, F.; Wada, Y.; Ohashi, N.; Cordier, S. From $Cs_2Mo_6Cl_{14}$ to $Cs_2Mo_6Cl_{14}{\cdot}H_2O$ and Vice Versa: Crystal Chemistry Investigations. *J. Cluster Sci.* **2017**, *28*, 773−798.
(47) Saito, N.; Wada, Y.; Lemoine, P.; Cordier, S.; Grasset, F.; Ohsawa, T.; Saito, N.; Cross, J. S.; Ohashi, N. Theoretical and Experimental Determination of the Crystal Structures of Cesium−Molybdenum Chloride. *Jpn. J. Appl. Phys.* **2016**, *55*, 075502.
(48) Johnston, D. H.; Agho, I. Crystal Structures and Hydrogen-Bonding Analysis of a Series of Solvated Ammonium Salts of Molybdenum(II) Chloride Clusters. *Acta Crystallogr. Sect. E* **2019**, *75*, 1705−1711.
(49) Saito, N.; Lemoine, P.; Cordier, S.; Wada, Y.; Ohsawa, T.; Saito, N.; Grasset, F.; Cross, J. S.; Ohashi, N. Solvent-Mediated Purification of Hexa-Molybdenum Cluster Halide, $Cs_2[Mo_6Cl_{14}]$ for Enhanced Optical Properties. *CrystEngComm* **2017**, *19*, 6028−6038.
(50) Saito, N.; Cordier, S.; Lemoine, P.; Ohsawa, T.; Wada, Y.; Grasset, F.; Cross, J.; Ohashi, N. Lattice and Valence Electronic Structures of Crystalline Octahedral Molybdenum Halide Clusters-Based Compounds, $Cs_2[Mo_6X_{14}]$ (X = Cl, Br, I), Studied by Density Functional Theory Calculations. *Inorg. Chem.* **2017**, *56*, 6234−6243.
(51) Saito, N.; Lemoine, P.; Cordier, S.; Ohsawa, T.; Wada, Y.; Grasset, F.; Cross, J. S.; Ohashi, N. Simulation of Crystal and Electronic Structures of Octahedral Molybdenum Cluster Complex Compound $Cs_2[Mo_6Cl_{14}]$ Using Various DFT Functionals. *J. Ceram. Soc. Jpn.* **2017**, *125*, 753−759.
(52) Czuchnowski, J.; Prevedel, R. Improving the Sensitivity of Planar Fabry−Pérot Cavities via Adaptive Optics and Mode Filtering. *Adv. Opt. Mater.* **2021**, *9*, 2001337.
(53) Hunger, D.; Steinmetz, T.; Colombe, Y.; Deutsch, C.; Hänsch, T. W.; Reichel, J. A Fiber Fabry−Perot Cavity with High Finesse. *New J. Phys.* **2010**, *12*, 65038.
(54) Islam, M.; Ali, M.; Lai, M.-H.; Lim, K.-S.; Ahmad, H. Chronology of Fabry-Perot Interferometer Fiber-Optic Sensors and Their Applications: A Review. *Sensors* **2014**, *14*, 7451−7488.
(55) Dobrovolsky, A.; Stehr, J. E.; Sukrittanon, S.; Kuang, Y.; Tu, C. W.; Chen, W. M.; Buyanova, I. A. Fabry−Perot Microcavity Modes in Single GaP/GaNP Core/Shell Nanowires. *Small* **2015**, *11*, 6331−6337.
(56) Li, J.; Jiang, M.; Xu, C.; Wang, Y.; Lin, Y.; Lu, J.; Shi, Z. Plasmon Coupled Fabry-Perot Lasing Enhancement in Graphene/ZnO Hybrid Microcavity. *Sci. Rep.* **2015**, *5*, 9263.
(57) Furchi, M.; Urich, A.; Pospischil, A.; Lilley, G.; Unterrainer, K.; Detz, H.; Klang, P.; Andrews, A. M.; Schrenk, W.; Strasser, G.; Mueller, T. Microcavity-Integrated Graphene Photodetector. *Nano Lett.* **2012**, *12*, 2773−2777.
(58) Fabre, B.; Cordier, S.; Molard, Y.; Perrin, C.; Ababou-Girard, S.; Godet, C. Electrochemical and Charge Transport Behavior of Molybdenum-Based Metallic Cluster Layers Immobilized on Modified n- and p-Type Si(111) Surfaces. *J. Phys. Chem. C* **2009**, *113*, 17437−17446.
(59) Ramiro-Manzano, F.; García-Aboal, R.; Fenollosa, R.; Biasi, S.; Rodriguez, I.; Atienzar, P.; Meseguer, F. Optical Properties of Organic/Inorganic Perovskite Microcrystals through the Characterization of Fabry−Pérot Resonances. *Dalt. Trans.* **2020**, *49*, 12798−12804.
(60) Saleh, B. E. A.; Teich, M. C. *Fundamentals of Photonics*, 2nd ed.; Wiley: New York, USA, 2007.
(61) Poelman, D.; Smet, P. F. Methods for the Determination of the Optical Constants of Thin Films from Single Transmission Measurements: A Critical Review. *J. Phys. D: Appl. Phys.* **2003**, *36*, 1850−1857.
(62) Sian, T. S.; Reddy, G. B. Optical, Structural and Photoelectron Spectroscopic Studies on Amorphous and Crystalline Molybdenum Oxide Thin Films. *Sol. Energy Mater. Sol. Cells* **2004**, *82*, 375−386.
(63) Vos, M. F. J.; Macco, B.; Thissen, N. F. W.; Bol, A. A.; Kessels, W. M. M. Atomic Layer Deposition of Molybdenum Oxide from (NtBu)2(NMe2)2Mo and O2 Plasma. *J. Vac. Sci. Technol., A* **2016**, *34*, 01A103.
(64) Szekeres, A.; Ivanova, T.; Gesheva, K. Spectroscopic Ellipsometry Study of CVD Molybdenum Oxide Films: Effect of Temperature. *J. Solid State Electrochem.* **2002**, *7*, 17−20.
(65) Deb, S. K.; Bowden, F. P. Physical Properties of a Transition Metal Oxide: Optical and Photoelectric Properties of Single Crystal and Thin Film Molybdenum Trioxide. *Proc. R. Soc. London. Ser. A. Math. Phys. Sci.* **1968**, *304*, 211−231.
(66) Ivanova, T.; Szekeres, A.; Gartner, M.; Gogova, D.; Gesheva, K. A. Spectroscopic Characterization of CVD-Molybdenum Oxide Films. *Electrochim. Acta* **2001**, *46*, 2215−2219.

https://doi.org/10.1021/acs.cgd.1c01144
Cryst. Growth Des. 2022, 22, 60−65